Nanoporous Block Copolymer Membranes for Ultrafiltration: A Simple Approach to Size Tunability

Hyungju Ahn,[†] Sungmin Park,[‡] Sang-Woo Kim,[‡] Pil J. Yoo,[§] Du Yeol Ryu,[*,‡] and Thomas P. Russell[*,∥,⊥]

[†]Department of Life Science & Chemical Materials, Pohang Accelerator Laboratory, POSTECH, 80 Jigok-ro, Nam-gu Pohang 790-834, Korea, [‡]Department of Chemical and Biomolecular Engineering, Yonsei University, 50 Yonsei-ro, Seodaemun-gu Seoul 120-749, Korea, [§]School of Chemical Engineering, SKKU Advanced Institute of Nanotechnology (SAINT), Sungkyunkwan University, Suwon 440-746, Korea, [∥]Polymer Science and Engineering Department, University of Massachusetts, Amherst, Massachusetts 01003, United States, and [⊥]WPI—Advanced Institute for Materials Research (WPI-AIMR), Tohoku University, 2-1-1 Katahira, Aoba, Sendai 980-8577, Japan

ABSTRACT Nanoporous structures were obtained by the self-assembly of polystyrene-*b*-poly(methyl methacrylate) (PS-*b*-PMMA) block copolymers (BCP) where, in thick films, cylindrical microdomains were oriented normal to the substrate and air interfaces, and in the interior of the films, the microdomains were randomly oriented. Continuous nanopores that penetrated through the film were readily produced by a simple preferential swelling of the PMMA microdomains. The confined swelling and rapid contraction of PMMA microdomains generated well-defined uniform pores with diameters to 17.5 nm. The size selectivity and rejection of Au nanoparticles (NPs) for these ultrafiltration (UF) membranes were demonstrated, suggesting an efficient route to tunable, noncomponent-degradative UF membranes.

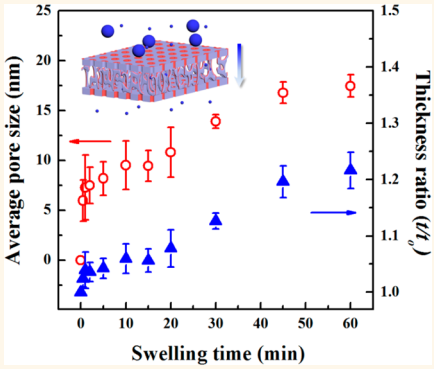

KEYWORDS: self-assembly · block copolymers · nanopores · ultrafiltration · membranes

Arrays of nanopores have widely been used as templates for high-surface area applications, like high-density storage media, catalysis, and ultrafiltration (UF) membranes.[1−5] Block copolymers (BCPs) can be used as nanopore-generating materials to produce templates and scaffolds for the fabrication of nanostructured materials, since dissimilar polymers linked together covalently self-assemble into the periodic arrays of lamellar, cylindrical, spherical, and gyroid morphologies with typical feature sizes of 10−50 nm and either one component can be selectively removed or phase selective chemistries can be used to generate the nanostructures.[2,6−11] For UF membrane applications, the self-assembly of BCPs presents an attractive approach for highly size-selective, permeable membranes due to their narrow size distributions and high pore densities.[4,12−15] There have been numerous attempts to achieve well-defined cylindrical or 3-dimensional nanostructures from BCP films so as to produce nanoscale porous media.[4,12−14,16−20] The diverse range of chemical structures available with BCPs provides unique opportunities to generate functional UF membranes for separation.[6,21−23]

Several studies on UF membranes based on the BCPs introduced different preparation strategies, like selective-etched monoliths, solvent evaporation, and nonsolvent-induced phase separation (NIPS). Cussler and co-workers used polylactide (PLA)-containing BCPs to generate porous templates that were prepared by shear-aligned monoliths or rapid solvent evaporation, followed by the selective hydrolysis of the PLA microdomains.[18,24,25] Peinemann, Abetz, and co-workers introduced a new type of nanoporous UF membranes using nonsolvent-induced phase separation with polystyrene-*b*-poly(4-vinylpridine) (PS-*b*-P4VP), in which the cylindrical channels were formed on the top of a random sponge-like layer that contains large porous structures.[20,26−28] The size selectivity and separation of biomolecules with these membranes could be controlled by the pH-responsive characteristics

* Address correspondence to dyryu@yonsei.ac.kr, russell@mail.pse.edu.

Received for review September 16, 2014 and accepted November 2, 2014.

Published online November 02, 2014
10.1021/nn505234v

© 2014 American Chemical Society

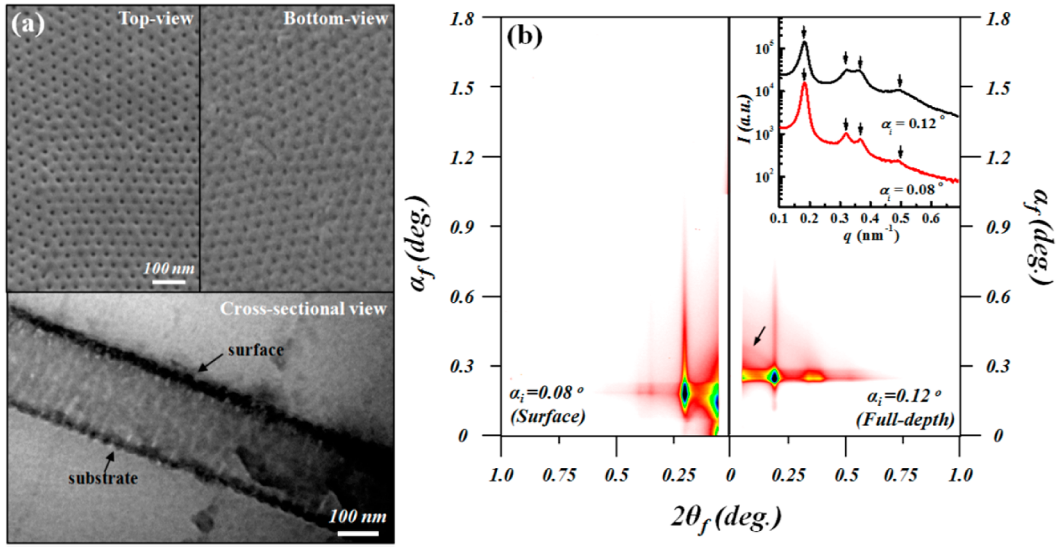

Figure 1. (a) Top and bottom-view SEM images and cross-sectional TEM image for UV-etched, nanoporous PS-*b*-PMMA film, in which the PMMA microdomains were entirely removed by the sequential UV exposure and acetic acid treatment. (b) 2-D GISAXS patterns for nanoporous PS-*b*-PMMA film, which were measured at incident angles of α_i = 0.08° (surface) and 0.12° (full-depth). The inset shows the line intensity scanned along the *in-plane* direction at α_f = 0.160° and 0.240° for surface and full-depth GISAXS patterns, respectively.

of P4VP. Kim and co-workers described the generation of nanoporous UF membranes from thin films by selective etching of the cylindrical PMMA microdomains, which showed the ability to isolate 30 nm-diameter human rhinovirus type 14 (HRV-14);[12,13] these works were derived from a surface reconstruction study on thin films of polystyrene-*b*-poly(methyl methacrylate) (PS-*b*-PMMA) by Russell and co-workers.[29] While these results demonstrate the ability to fabricate nanoporous UF membranes from self-assembled BCP morphologies, achieving tunability in the pore size, relevant to separations of a large range of biomolecules and chemical species, is still a challenge.[15,20,28,30] Moreover, a key issue has been to avoid component-degradative routes that deteriorate in mechanical stability, while maintaining membrane performance.

Here, we used thick films of a thermally annealed PS-*b*-PMMA on substrates with balanced interfacial interactions to produce the films with the microdomains oriented normal to the substrate and air interfaces but randomly oriented in the interior of the films. Using only a selective solvent for the PMMA comprising the cylindrical microdomains, a simple swelling of the PMMA microdomains followed by rinsing with deionized (DI) water, led to nanopores that penetrated through the film, resulting in UF membrane with pores ranging from 6.0 to 17.5 nm in diameter having exceptional size selectivity for Au NPs. These results demonstrate a simple route to generate tunable, nanoporous UF membranes with no film or component degradation process.

RESULTS AND DISCUSSION

A 200 nm-thick (~$6L_o$, where L_o is the repeat period of the cylindrical microdomains in the bulk) PS-*b*-PMMA film was spin coated onto a neutral substrate, having a random copolymer of S and MMA anchored to the surface to balance interfacial interactions, and thermally annealed at 180 °C for 2 days under vacuum. Figure 1a shows SEM images of the top and bottom, and a cross-sectional TEM image of a film. To enhance the phase contrast by the difference in electron density, the PMMA block was entirely removed by the sequential UV irradiation (λ = 254 nm) and washing with acetic acid. The top and bottom show hexagonally packed pores with a diameter of ~21 nm, while the cross-section shows cylindrical pores oriented normal to the substrate and air interfaces and random arrangement of the pores in the interior. The film was characterized by grazing incidence small-angle X-ray scattering (GISAXS), as shown in Figure 1b. In the GISAXS geometry, α_f and $2\theta_f$ are the exit angles of the X-ray beam in the *out-of-plane* direction (i.e., normal to the sample surface) and in the *in-plane* direction (i.e., parallel to the sample surface), respectively, where $q = (4\pi/\lambda)\sin\theta_f$ is the scattering vector. The GISAXS at which (α_i = 0.08°, denoted as surface) is less than the critical angle (α_c = 0.10°) shows intense, multiple-order Bragg-rod peaks at scattering vector ratios of $q/q^* = 1{:}\sqrt{3}{:}\sqrt{4}{:}\sqrt{7}$ (as shown in the inset), indicating hexagonally packed pores at the surface, in agreement with the SEM images in Figure 1a. For an incidence angle above the critical angle (here shown for α_i = 0.12°, denoted as full-depth) the X-rays penetrate through the entire sample, the Bragg-rod scattering from the surface is evident and is superposed on a diffuse elliptical scattering (marked with arrow) which is consistent with pores initially being orthogonal to the surface and then randomly oriented in the interior

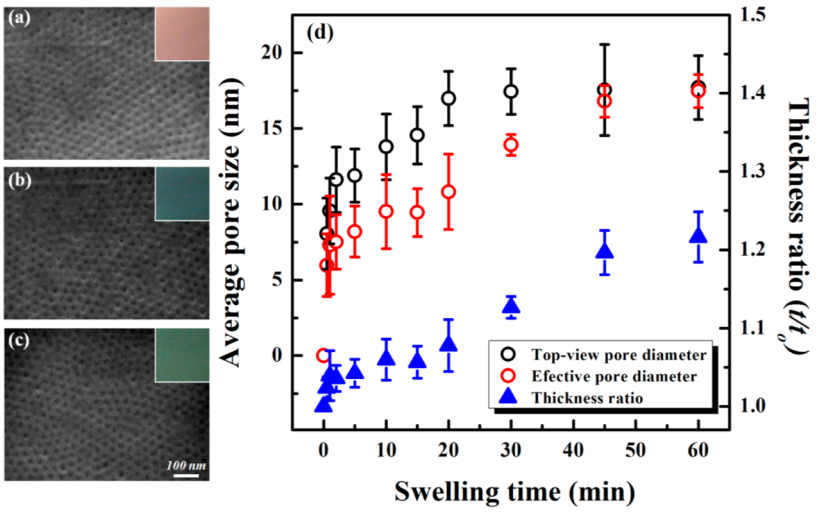

Figure 2. SEM images for nanoporous PS-*b*-PMMA films with swelling time of (a) 30 s, (b) 2 min, and (c) 60 min in acetic acid, where the insets show OM images reflecting the changes in film thickness. (d) Average pore size (or diameter) and thickness ratio (t/t_o) for nanoporous PS-*b*-PMMA films as a function of swelling time in acetic acid. The diameters were evaluated from the top-view SEM images (on the film surface) and calculated with thickness as the effective pore size (D).

of the films in minor. This is, also, consistent with the images in Figure 1. The ellipticity of the pattern indicates that the average center-to-center distance in the plane of the film is smaller than that normal to the surface.

The interfacial interactions between the blocks of the PS-*b*-PMMA and the substrate were balanced, and the surface energies of the PS and PMMA blocks are essentially equal at the annealing temperature, which give rise to the orientation of the microdomains normal to the interfaces. However, as shown in previous studies, this orientation dissipates with distance from the interface, leading to the randomly oriented PMMA cylinders in the interior of the films.[13] This random orientation of the PMMA cylindrical microdomains is expected to impart isotropic mechanical stability to the films, as opposed to the case with unidirectionally aligned cylindrical microdomains. From the position of the maximum in the scattering ($q^* = 0.183$ nm^{-1}), an average center-to-center distance in the plane of the film was 34.3 nm, as calculated from $d = 2\pi/q^*$. The average diameter (D_{PMMA}) of the PMMA cylindrical microdomains was calculated to be 20.8 nm by

$$D_{PMMA} = \frac{4d}{\sqrt{3}}\left[\frac{\sqrt{3}}{2\pi}(1 - \phi_{PS})\right]^{0.5} \quad (1)$$

where d and ϕ_{PS} are the d-spacing of PMMA cylindrical microdomains in the plane of the film and the volume fraction of the PS matrix, respectively (Supporting Information, Figure S1). This is in excellent agreement with the average pore diameter (~21 nm) determined from the top-view SEM image for a UV-etched, nanoporous film in Figure 1a.

To tune the diameter of the pores, the cylindrical PMMA microdomains in the glassy PS matrix were swollen with acetic acid, a good solvent for PMMA, for different periods of time. Subsequently, the acetic acid was immediately removed by rinsing with DI water. Hexagonally packed pores were generated in the dried BCP films, as shown by the top-view SEM images in Figure 2a–c. The pore diameters on the film surface were measured to be 8, 11, and 18 nm with swelling time of 30 s, 2 min, and 60 min, respectively. Figure 2d shows the average pore size (or diameter) and thickness ratio (t/t_o) as a function of swelling time in acetic acid, where the pore sizes were evaluated from the top-view SEM images and calculated with thickness. Upon swelling in acetic acid for 20 min, the top-view pore diameter increased significantly from 8 nm at 30 s to 18 nm, but with further swelling time it remained at a limiting value of 18 nm due to a swelling equilibrium between mixing and elastic energies. The film thickness of the dried sample increased by 21.6% after swelling process for 60 min, although acetic acid is not a good solvent for the PS matrix. The color change in the films, as shown by optical microscopy (OM) in the insets, reflects the change in the film thickness. When the PS-*b*-PMMA films were in contact with acetic acid, the solvent solubilized the PMMA chains, causing the microdomains to swell in the glassy PS matrix. The osmotic force associated with the solubilization of the PMMA was sufficiently large to cause a finite plasticization of the PS matrix. However, in the plane of the film, due to the confinement of the film by the boundaries of the substrate, the average center-to-center distance remained constant (Supporting Information, Figure S2). Removal of the solvent from the microdomains in the still-glassy matrix gave rise to the formation of the pores, where the size of pores was dictated by the amount of solvent taken up by the PMMA. Therefore, an increase in film

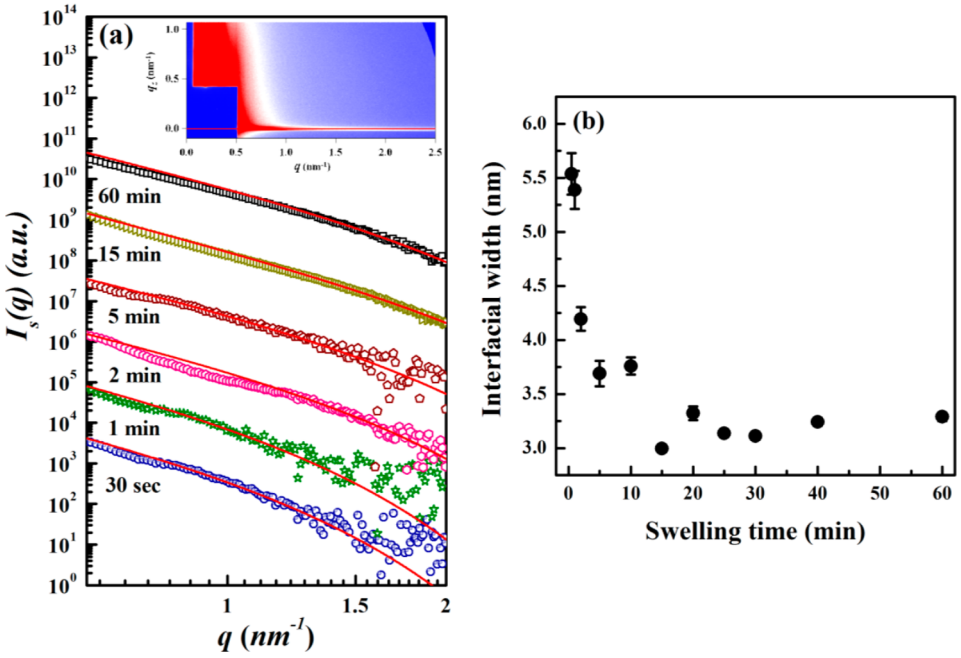

Figure 3. (a) The *in-plane* scattering intensity ($I_s(q)$) from the high-*q* GISAXS for nanoporous PS-*b*-PMMA films, for which the swelling time in acetic acid was varied. Each red line was obtained by the linear fit from the Porod plot. The plots were shifted upward by a factor of 3 to avoid overlapping. The inset shows the high-*q* GISAXS image for nanoporous PS-*b*-PMMA film with swelling time of 5 min. (b) Interfacial width (*w*) between polymer and air as a function of swelling time.

thickness normal to the surface with a selective solvent is associated with the volume increase of the continuous nanopores, enabling calculation of the effective pore size (*D*) assuming a regular hexagon as a unit cell,

$$D = \sqrt{\frac{4}{3\pi} S\left(1 - \frac{t_o}{t}\right)} \quad (2)$$

where *S* is the surface area of unit cell, and t_o and *t* are initial and swollen film thicknesses, respectively (Supporting Information, Figure S1). The effective pore size (*D*), hereafter referred to as the pore size, rapidly increased from 6.0 nm at 30 s to 17.5 nm at 60 min, which would be more accurate than the top-view pore size, as displayed by the red color in Figure 2d. These results show that the pore size of the BCP films can be simply controlled by the time allowed for swelling. A particularly attractive feature of this approach is that the BCP chains are left intact and the mechanical strength of the film is retained.

To quantify the change in the pore diameter during the confined swelling of PMMA microdomains in the PS matrix, a Porod analysis was performed on the scattered intensity at high-*q* GISAXS. For a two-phase system having infinitely sharp phase boundaries,[31]

$$\lim_{q \to \infty} I_p(q) = \frac{K}{q^4} \quad (3)$$

where *K* is the Porod constant dictated by the electron density contrast between the domains (proportional to the total integrated scattering) and total surface area between two phases in the scattering volume, and $I_p(q)$ is the scattering for this idealized system. In general, interfaces are not infinitely sharp and can be described by a sigmoidal function, obtained by convoluting a step function with a Gaussian having a full width at half-maximum of σ. This broadened interface causes the scattering to decrease more rapidly than q^{-4} by an amount given by $\exp(-\sigma^2 q^2)$. In addition, thermal density fluctuations give rise to a constant level of scattering or background ($I_B(q)$) that must be subtracted from the observed scattering, as given by

$$I_S(q) = I_{obs}(q) - I_B(q) = I_p(q) \exp(-\sigma^2 q^2) \quad (4)$$

Consequently, from a plot of $\ln(q^4 I_s(q))$ *vs* q^2, σ can be determined and the interfacial width (*w*), related to the interfacial energy between the domains, can be obtained by[32,33]

$$w = \sqrt{2\pi}\sigma \quad (5)$$

Figure 3a shows *in-plane* scattering intensity ($I_s(q)$) for nanoporous PS-*b*-PMMA films as a function of scattering vector (*q*), where the low-*q* region from 0 to 0.519 nm^{-1} was blocked to enhance the signal-to-noise of the scattering intensity at high *q*. Fits to the data using eqs 2 and 3 are shown in Figure 3b, and the variation in the interfacial width as a function of swelling time is shown. Initially, a large value (5.54 ± 0.19 nm) was caused by partial and irregular swelling at the early stage (30 s) and rapid contraction of PMMA microdomains during rinsing with DI water, producing the nanoporous BCP film with a pore diameter of 6.0 nm. As the solvent penetrates and solubilizes the

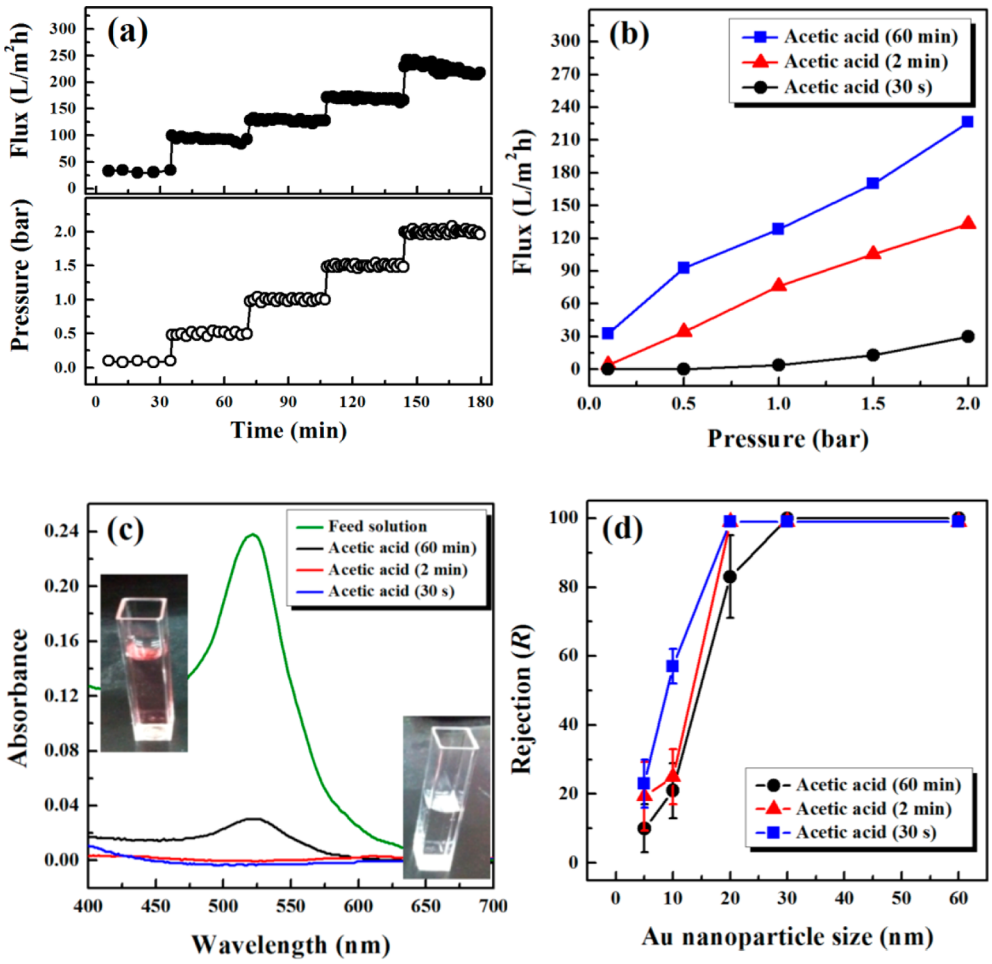

Figure 4. (a) Flux of deionized (DI) water for 200 nm-thick, nanoporous PS-*b*-PMMA film with a swelling time of 60 min in acetic acid, where the pressure was step-wisely applied from 0.1 to 2.0 bar. (b) Pressure-dependent flux for nanoporous PS-*b*-PMMA films with swelling time of 30 s, 2 min, and 60 min in acetic acid (corresponding to pore diameters of 6.0, 7.5, and 17.5 nm, respectively). (c) UV−vis absorption spectra of feed solution with 20 nm Au NPs and filtered solution through nanoporous PS-*b*-PMMA films with swelling times of 30 s, 2 min, and 60 min. (d) Rejection (*R*) of nanoporous UF membranes as a function of Au NP size.

PMMA, the effective interactions become more nonfavorable and the interface narrowed from the inherent interfacial width between the two blocks (~5 nm).[33,34] In addition, for the porous films, the only interface of relevance is that between PMMA and air. Consequently, the interfacial width decreases to 3.3 ± 0.06 nm and remains constant at that value with increasing pore diameter; this well-defined interface is crucial for their narrow size distributions and highly uniform porosity of nanoporous membranes.

BCP films for the membrane were simply prepared on a neutral substrate with a thick native oxide layer. The nanoporous membrane was removed from the substrate using a 5 wt % HF solution and transferred onto a macroporous PVDF membrane to produce a composite UF membrane.[12,13] Figure 4a shows the performance of an 17.5 nm-diameter nanoporous PS-*b*-PMMA membrane that was prepared with swelling time of 60 min by measuring the flux of DI water with a stepwise increase in the applied pressure (from 0.1 to 2.0 bar). Figure 4b shows the pressure-dependent flux for different pore diameters (corresponding to different swelling times). Throughout these measurements the membranes were undamaged. At a constant pressure, the flux of the nanoporous PS-*b*-PMMA membranes increased with increasing swelling time in acetic acid due to an increase in porosity. The porosities of BCP membranes with swelling times of 30 s, 2 min, and 60 min were calculated to be 2.1, 3.3, and 17.7%, respectively. However, the flux (128 L/(m^2 h) at 1 bar) of BCP membrane with a swelling time of 60 min is comparable to that (195 L/(m^2 h)) of conventional poly(ether sulfone) (PES) UF membrane,[35] although the porosity (17.7%) of the membrane was low.

Au NP dispersions in DI water were used to measure the size selectivity and rejection of BCP UF membranes at a constant pressure of 1 bar. Figure 4c shows UV−vis absorption spectra of the feed with 20 nm (in diameter) Au NPs and the filtrate through the BCP membranes with swelling times of 30 s, 2 min, and 60 min, corresponding to pore diameters of 6.0, 7.5, and 17.5 nm, respectively. A maximum in the UV−vis absorption at

520 nm corresponded to the characteristic absorbance of 20 nm Au NPs. For BCP membranes with a pore diameter of 17.5 nm, the absorbance at 520 nm decreased by 87.4%. Given the size dispersity of the original NPs (from 16 to 24 nm provided by manufacturer), the results indicate that 20 nm Au NPs were effectively rejected by the membrane. For BCP membranes with swelling times of 30 s and 2 min, the absorbance at 520 nm disappeared completely and the color associated with the NPs (Figure 4c) vanished, indicating a total rejection of the NPs. Figure 4d shows the overall rejection (R) of nanoporous BCP UF membranes as a function of Au NP size. The relative rejection of the Au NPs was calculated by

$$R\% = \left(1 - \frac{A_f}{A_o}\right)100 \quad (5)$$

where A_o and A_f denote the absorbance of feed and filtered solutions, respectively.

All Au NPs over 30 nm were rejected by all the BCP membranes considered here, the nanoporous PS-*b*-PMMA films with swelling times of 30 s, 2 min, and 60 min. For 5 nm and 10 nm Au NPs, the nanoporous BCP membranes with a swelling time of 30 s (having pore diameters of 6.0 nm) showed a 57% rejection of 10 nm Au NPs, although with other films, this was less than 25%. Furthermore, even the regenerated BCP membrane that underwent acid and base washing showed consistent membrane performance (Supporting Information, Figure S3).

CONCLUSIONS

The results presented above demonstrate that by only controlling the orientation of the BCP cylindrical microdomains at both interfaces, thick nanoporous ultrafiltration membranes can easily be produced by a simple swelling of the minor component in a matrix that remains glassy. Using only a selective solvent for the PMMA comprising the cylindrical microdomains, the confined swelling and rapid contraction of PMMA microdomains generated highly uniform nanopores that penetrated through the film. The interfaces between pore walls (or PMMA) and air in the nanoporous structures were developed to the interfacial width of 3.3 $\pm$ 0.06 nm for high pore regularity, resulting in an UF membrane with pores ranging from 6.0 to 17.5 nm in diameter.

Excellent size selectivity with high rejection of Au NPs was achieved at high pressures to 2 bar. In addition, the membranes were found to be resistant to acid and base washing required for regeneration and had excellent mechanical stability. The nondegradative approach with highly uniform porosity described here was scaled up to 4-in.-diameter nanoporous membrane films (Supporting Information, Figure S4), suggesting a possible route for fabricating tunable UF membranes in a large scale.

METHODS

Materials. A cylinder-forming PS-*b*-PMMA copolymer was synthesized by sequential anionic polymerization of styrene and methyl methacrylate in tetrahydrofuran (THF) solvent; this was performed at −78 °C in the presence of LiCl (high purity, Aldrich), under purified argon. A *sec*-butyllithium was used as an initiator. The number-averaged molecular-weight (M_n), as characterized by size-exclusion chromatography (SEC), was 73 000 g/mol with a narrow dispersity of 1.05. PS volume fraction (ϕ_{PS}) was determined to be 0.751 by ^{1}H nuclear magnetic resonance (^{1}H NMR), based on the mass densities of the two components (1.05 and 1.184 g/cm^3 for PS and PMMA, respectively). A neutral substrate was prepared using a hydroxyl end-functionalized poly(styrene-*r*-methyl methacrylate) (HO-P(S-*r*-MMA)) with a styrene mole fraction (X_S) ~ 0.64 and M_n = 10 000 g/mol with a dispersity of 1.30.[36]

Preparation of Nanoporous BCP Membranes. PS-*b*-PMMA films were prepared by spin-coating (5.5 wt % solutions typically at 4000 rpm for 60 s) on a neutral substrate by HO-P(S-*r*-MMA) that was anchored to the substrate, where the brush thickness of P(S-*r*-MMA) was measured to be ~4.6 $\pm$ 0.2 nm by ellipsometry (SE MG-1000, Nanoview) at an incidence angle of 70° after rinsing with toluene to remove the unreacted polymer chains from the substrate. The 200 nm-thick ($\approx 6L_o$) BCP films were sequentially annealed at 180 °C for 2 days under vacuum. To prepare the nanoporous structures, PS-*b*-PMMA films were simply immersed into the acetic acid for different periods of time, followed by thoroughly rinsing with DI water for 30 min and drying in ambient condition for longer than 3 h. The dried PS-*b*-PMMA films were floated to the surface of a 5 wt % HF solution then transferred to a porous poly(vinylidene fluoride) (PVDF) supporting membrane with an average pore diameter of 0.22 μm (Millipore). For the UV etch process, the BCP films were exposed to UV for 1 h under vacuum before acetic acid treatment.

Characterization of BCP Films. Grazing-incidence small-angle X-ray scattering (GISAXS) experiments were performed at the 9A beamline in Pohang Accelerator Laboratory (PAL), Korea and Beamline 7.3.3 in the Advanced Light Source (ALS), Lawrence Berkeley National Laboratory, USA. The operating conditions were chosen as a wavelength of 1.18 Å and a sample-to-detector distance of 2.92 m. To probe surface and internal structures of BCP films, the incidence angle (α_i) was varied from 0.08° to 0.14°. 2D-GISAXS patterns were recorded by using a CCD detector (Mar-165, Rayonix L.L.C.) positioned at the end of a vacuum guide tube with an exposure time of 10 s. Field emission scanning electron microscopy (FE-SEM; JSM-6701F, JEOL) was operated with an accelerating voltage of 5.0 kV using a semi-in-lens detector to examine the surface, bottom, and cross-view images of PS-*b*-PMMA films. Transmission electron microscopy (TEM; JEM-2010, JEOL) was done with an accelerating voltage of 200 kV to observe the morphology. Ultrathin specimens were prepared at −25 °C using a cryo-ultramicrotome (CRX-PTXL, RMC) with a diamond knife, where the PS block in the films was selectively stained with RuO_4 at room temperature to enhance the electron density contrast between two phases.

Permeability and Size Selectivity of Nanoporous UF Membranes. A homemade UF membrane cell was devised to measure the permeability of DI water and size selectivity at room temperature; this cell has a 10-mL working volume and an effective membrane area of 0.636 cm^2. Au NPs solutions with different sizes of diameter from 5 to 60 nm (Sigma-Aldrich) were filtered through nanoporous BCP films to characterize size

selectivity of the UF membranes, where the concentrations of Au NPs in feed and filtered solutions were analyzed by UV−vis absorption spectra.

Conflict of Interest: The authors declare no competing financial interest.

Supporting Information Available: Line intensity scanned along the *in-plane* direction at $\alpha_f = 0.160°$ from GISAXS patterns for nanoporous PS-*b*-PMMA film, where the swelling time in acetic acid was varied (Figure S2). Filtration performance of a regenerated PS-*b*-PMMA film with a swelling time of 2 min (Figure S3). A 4-in.-diameter nanoporous BCP film with swelling time of 60 min (Figure S4). This material is available free of charge *via* the Internet at http://pubs.acs.org.

Acknowledgment. This work was supported by the U.S. Department of Energy BES under contract BES-DE-FG02-96ER45612 and by a grant from Innovaprep. Some of the GISAXS measurements were performed at the 7.3.3 beamline at the Advanced Light Source, Lawrence Berkeley National Laboratory, which is supported by the Office of Science, Office of Basic Energy Sciences, of the U.S. Department of Energy under Contract No. DE-AC02-05ch11231. This work was also supported by the supports from NRF (Grants 2014R1A2A2A01004364, 2014M3C1A3053035) and APCPI ERC (R11-2007-050-00000), funded by the Ministry of Education, Science & Technology (MEST), Korea.

REFERENCES AND NOTES

1. Park, M.; Harrison, C.; Chaikin, P. M.; Register, R. A.; Adamson, D. H. Block Copolymer Lithography: Periodic Arrays of 10^{11} Holes in 1 Square Centimeter. *Science* **1997**, *276*, 1401–1404.
2. Thurn-Albrecht, T.; Schotter, J.; Kastle, C. A.; Emley, N.; Shibauchi, T.; Krusin-Elbaum, L.; Guarini, K.; Black, C. T.; Tuominen, M. T.; Russell, T. P. Ultrahigh-Density Nanowire Arrays Grown in Self-Assembled Diblock Copolymer Templates. *Science* **2000**, *290*, 2126–2129.
3. Bang, J.; Jeong, U.; Ryu, D. Y.; Russell, T. P.; Hawker, C. J. Block Copolymer Nanolithography: Translation of Molecular Level Control to Nanoscale Patterns. *Adv. Mater.* **2009**, *21*, 4769–4792.
4. Jackson, E. A.; Hillmyer, M. A. Nanoporous Membranes Derived from Block Copolymers: From Drug Delivery to Water Filtration. *ACS Nano* **2010**, *4*, 3548–3553.
5. Herr, D. J. C. Directed Block Copolymer Self-Assembly for Nanoelectronics Fabrication. *J. Mater. Res.* **2011**, *26*, 122–139.
6. Hashimoto, T.; Tsutsumi, K.; Funaki, Y. Nanoprocessing Based on Bicontinuous Microdomains of Block Copolymers: Nanochannels Coated with Metals. *Langmuir* **1997**, *13*, 6869–6872.
7. Chan, V. Z.-H.; Hoffman, J.; Lee, V. Y.; Iatrou, H.; Avgeropoulos, A.; Hadjichristidis, N.; Miller, R. D.; Thomas, E. L. Ordered Bicontinuous Nanoporous and Nanorelief Ceramic Films from Self Assembling Polymer Precursors. *Science* **1999**, *286*, 1716–1719.
8. Wang, Y.; Gösele, U.; Steinhart, M. Mesoporous Polymer Nanofibers by Infiltration of Block Copolymers with Sacrificial Domains into Porous Alumina. *Chem. Mater.* **2007**, *20*, 379–381.
9. Crossland, E. J. W.; Nedelcu, M.; Ducati, C.; Ludwigs, S.; Hillmyer, M. A.; Steiner, U.; Snaith, H. J. Block Copolymer Morphologies in Dye-Sensitized Solar Cells: Probing the Photovoltaic Structure−Function Relation. *Nano Lett.* **2008**, *9*, 2813–2819.
10. Crossland, E. J. W.; Kamperman, M.; Nedelcu, M.; Ducati, C.; Wiesner, U.; Smilgies, D. M.; Toombes, G. E. S.; Hillmyer, M. A.; Ludwigs, S.; Steiner, U.; Snaith, H. J. A Bicontinuous Double Gyroid Hybrid Solar Cell. *Nano Lett.* **2008**, *9*, 2807–2812.
11. Hsueh, H.-Y.; Chen, H.-Y.; She, M.-S.; Chen, C.-K.; Ho, R.-M.; Gwo, S.; Hasegawa, H.; Thomas, E. L. Inorganic Gyroid with Exceptionally Low Refractive Index from Block Copolymer Templating. *Nano Lett.* **2010**, *10*, 4994–5000.
12. Yang, S. Y.; Ryu, I.; Kim, H. Y.; Kim, J. K.; Jang, S. K.; Russell, T. P. Nanoporous Membranes with Ultrahigh Selectivity and Flux for the Filtration of Viruses. *Adv. Mater.* **2006**, *18*, 709–712.
13. Yang, S. Y.; Park, J.; Yoon, J.; Ree, M.; Jang, S. K.; Kim, J. K. Virus Filtration Membranes Prepared from Nanoporous Block Copolymers with Good Dimensional Stability under High Pressures and Excellent Solvent Resistance. *Adv. Funct. Mater.* **2008**, *18*, 1371–1377.
14. Uehara, H.; Kakiage, M.; Sekiya, M.; Sakuma, D.; Yamonobe, T.; Takano, N.; Barraud, A.; Meurville, E.; Ryser, P. Size-Selective Diffusion in Nanoporous but Flexible Membranes for Glucose Sensors. *ACS Nano* **2009**, *3*, 924–932.
15. Wang, Y.; Li, F. An Emerging Pore-Making Strategy: Confined Swelling-Induced Pore Generation in Block Copolymer Materials. *Adv. Mater.* **2011**, *23*, 2134–2148.
16. Olson, D. A.; Chen, L.; Hillmyer, M. A. Templating Nanoporous Polymers with Ordered Block Copolymers. *Chem. Mater.* **2007**, *20*, 869–890.
17. Nuxoll, E. E.; Hillmyer, M. A.; Wang, R.; Leighton, C.; Siegel, R. A. Composite Block Polymer−Microfabricated Silicon Nanoporous Membrane. *ACS Appl. Mater. Interfaces* **2009**, *1*, 888–893.
18. Phillip, W. A.; O'Neill, B.; Rodwogin, M.; Hillmyer, M. A.; Cussler, E. L. Self-Assembled Block Copolymer Thin Films as Water Filtration Membranes. *ACS Appl. Mater. Interfaces* **2010**, *2*, 847–853.
19. Yang, S. Y.; Yang, J.-A.; Kim, E.-S.; Jeon, G.; Oh, E. J.; Choi, K. Y.; Hahn, S. K.; Kim, J. K. Single-File Diffusion of Protein Drugs through Cylindrical Nanochannels. *ACS Nano* **2010**, *4*, 3817–3822.
20. Qiu, X.; Yu, H.; Karunakaran, M.; Pradeep, N.; Nunes, S. P.; Peinemann, K.-V. Selective Separation of Similarly Sized Proteins with Tunable Nanoporous Block Copolymer Membranes. *ACS Nano* **2012**, *7*, 768–776.
21. Akthakul, A.; Salinaro, R. F.; Mayes, A. M. Antifouling Polymer Membranes with Subnanometer Size Selectivity. *Macromolecules* **2004**, *37*, 7663–7668.
22. Rzayev, J.; Hillmyer, M. A. Nanoporous Polystyrene Containing Hydrophilic Pores from an ABC Triblock Copolymer Precursor. *Macromolecules* **2004**, *38*, 3–5.
23. Schacher, F.; Ulbricht, M.; Müller, A. H. E. Self-Supporting, Double Stimuli-Responsive Porous Membranes from Polystyrene-block-poly(*N*,*N*-dimethylaminoethyl methacrylate) Diblock Copolymers. *Adv. Funct. Mater.* **2009**, *19*, 1040–1045.
24. Phillip, W. A.; Rzayev, J.; Hillmyer, M. A.; Cussler, E. L. Gas and Water Liquid Transport through Nanoporous Block Copolymer Membranes. *J. Mater. Sci.* **2006**, *286*, 144–152.
25. Phillip, W. A.; Amendt, M.; O'Neill, B.; Chen, L.; Hillmyer, M. A.; Cussler, E. L. Diffusion and Flow across Nanoporous Polydicyclopentadiene-Based Membranes. *ACS Appl. Mater. Interfaces* **2009**, *1*, 472–480.
26. Peinemann, K.-V.; Abetz, V.; Simon, P. F. W. Asymmetric Superstructure Formed in a Block Copolymer *via* Phase Separation. *Nat. Mater.* **2007**, *6*, 992–996.
27. Nunes, S. P.; Sougrat, R.; Hooghan, B.; Anjum, D. H.; Behzad, A. R.; Zhao, L.; Pradeep, N.; Pinnau, I.; Vainio, U.; Peinemann, K.-V. Ultraporous Films with Uniform Nanochannels by Block Copolymer Micelles Assembly. *Macromolecules* **2010**, *43*, 8079–8085.
28. Nunes, S. P.; Behzad, A. R.; Hooghan, B.; Sougrat, R.; Karunakaran, M.; Pradeep, N.; Vainio, U.; Peinemann, K.-V. Switchable pH-Responsive Polymeric Membranes Prepared *via* Block Copolymer Micelle Assembly. *ACS Nano* **2011**, *5*, 3516–3522.
29. Xu, T.; Stevens, J.; Villa, J. A.; Goldbach, J. T.; Guarini, K. W.; Black, C. T.; Hawker, C. J.; Russell, T. P. Block Copolymer Surface Reconstruction: A Reversible Route to Nanoporous Films. *Adv. Funct. Mater.* **2003**, *13*, 698–702.
30. Jeon, G.; Yang, S. Y.; Byun, J.; Kim, J. K. Electrically Actuatable Smart Nanoporous Membrane for Pulsatile Drug Release. *Nano Lett.* **2011**, *11*, 1284–1288.
31. Roe, R. J. *Method of X-rays and Neutron Scattering in Polymer Science*; Oxford University Press: 2000.
32. Hashimoto, T.; Todo, A.; Itoi, H.; Kawai, H. Domain-Boundary Structure of Styrene-Isoprene Block Copolymer Films Cast

from Solutions. 2. Quantitative Estimation of the Interfacial Thickness of Lamellar Microphase Systems. *Macromolecules* **1977**, *10*, 377–384.
33. Anastasiadis, S. H.; Russell, T. P.; Satija, S. K.; Majkrzak, C. F. The Morphology of Symmetric Diblock Copolymers as Revealed by Neutron Reflectivity. *J. Chem. Phys.* **1990**, *92*, 5677–5691.
34. Anastasiadis, S. H.; Russell, T. P.; Satija, S. K.; Majkrzak, C. F. Neutron Reflectivity Studies of The Surface-Induced Ordering of Diblock Copolymer Films. *Phys. Rev. Lett.* **1989**, *62*, 1852–1855.
35. Peeva, P. D.; Million, N.; Ulbricht, M. Factors Affecting the Sieving Behavior of Anti-fouling Thin-Layer Cross-Linked Hydrogel Polyethersulfone Composite Ultrafiltration Membranes. *J. Membr. Sci.* **2012**, *390−391*, 99–112.
36. Ham, S.; Shin, C.; Kim, E.; Ryu, D. Y.; Jeong, U.; Russell, T. P.; Hawker, C. J. Microdomain Orientation of PS-*b*-PMMA by Controlled Interfacial Interactions. *Macromolecules* **2008**, *41*, 6431–6437.